PROCEEDINGS B

royalsocietypublishing.org/journal/rspb

Research

Cite this article: Schrock SAR *et al*. 2025 Do fungi look like macroparasites? Quantifying the patterns and mechanisms of aggregation for host–fungal parasite relationships. *Proc. R. Soc. B* **292**: 20242013.
https://doi.org/10.1098/rspb.2024.2013

Received: 21 August 2024
Accepted: 13 January 2025

Subject Category:
Ecology

Subject Areas:
ecology, health and disease and epidemiology

Keywords:
aggregation, fungal parasites/pathogens, distribution, Batrachochytrium dendrobatidis, amphibian, integral projection model

Author for correspondence:
Sarah A. R. Schrock
e-mail: sschroc2@tennessee.edu

Electronic supplementary material is available online at https://doi.org/10.6084/m9.figshare.c.7667272.

THE ROYAL SOCIETY PUBLISHING

Do fungi look like macroparasites? Quantifying the patterns and mechanisms of aggregation for host–fungal parasite relationships

Sarah A. R. Schrock[1], Jason C. Walsman[2], Joseph DeMarchi[1], Emily H. LeSage[4], Michel E. B. Ohmer[5], Louise A. Rollins-Smith[6,7], Cheryl J. Briggs[2], Corinne L. Richards-Zawacki[8], Douglas C. Woodhams[9], Roland A. Knapp[10,3], Thomas C. Smith[10,3], Célio F. B. Haddad[11], C. Guilherme Becker[12,13], Pieter T. J. Johnson[14] and Mark Q. Wilber[1]

[1]School of Natural Resources, University of Tennessee Institute of Agriculture, Knoxville, TN, USA
[2]Ecology, Evolution, and Marine Biology, and [3]Earth Research Institute, University of California, Santa Barbara, CA, USA
[4]Biology Department, Skidmore College, Saratoga Springs, NY, USA
[5]Department of Biology, University of Mississippi, University Park, MS, USA
[6]Department of Pathology, Microbiology, and Immunology, Vanderbilt University School of Medicine, Nashville, TN, USA
[7]Department of Biological Sciences, Vanderbilt University, Nashville, TN, USA
[8]Department of Biological Sciences and Pymatuning Laboratory of Ecology, University of Pittsburgh, Pittsburgh, PA, USA
[9]Department of Biology, University of Massachusetts, Boston, MA, USA
[10]Sierra Nevada Aquatic Research Laboratory, University of California, Mammoth Lakes, CA, USA
[11]Department of Biodiversity and Aquaculture Center (CAUNESP), Universidade Estadual Paulista, Rio Claro, SP, Brazil
[12]Department of Biology, and [13]One Health Microbiome Center, Center for Infectious Disease Dynamics, Ecology Institute, Huck Institutes of the Life Sciences, The Pennsylvania State University, University Park, PA, USA
[14]Ecology and Evolutionary Biology, University of Colorado Boulder, Boulder, CO, USA

SARS, 0000-0001-5112-1687; JCW, 0000-0001-8141-0340; LAR-S, 0000-0002-5209-2459; TCS, 0000-0001-7908-438X; PTJJ, 0000-0002-7997-5390

Most hosts contain few parasites, whereas few hosts contain many. This pattern, known as aggregation, is well-documented in macroparasites where parasite intensity distribution among hosts affects host–parasite dynamics. Infection intensity also drives fungal disease dynamics, but we lack a basic understanding of host–fungal aggregation patterns, how they compare with macroparasites and if they reflect biological processes. To begin addressing these gaps, we characterized aggregation of the fungal pathogen *Batrachochytrium dendrobatidis* (Bd) in amphibian hosts. Using the slope of Taylor's Power law, we found Bd intensity distributions were more aggregated than many macroparasites, conforming closely to lognormal distributions. We observed that Bd aggregation patterns are strongly correlated with known biological processes operating in amphibian populations, such as epizoological phase (i.e. invasion, post-invasion and enzootic), and intensity-dependent disease mortality. Using intensity-dependent mathematical models, we found evidence of evolution of host resistance based on aggregation shifts in systems persisting with Bd following disease-induced declines. Our results show that Bd aggregation is highly conserved across disparate systems and contains signatures of potential biological processes of amphibian–Bd systems. Our work can inform future modelling approaches and be extended to other fungal pathogens to elucidate host–fungal interactions and unite host–fungal dynamics under a common theoretical framework.

1. Introduction

One of the few general laws of parasitology is that many hosts have few parasites, and few hosts have many parasites [1]. Known as 'aggregation', this pattern has important implications for the dynamics of host–parasite systems and our ability to infer the dominant processes operating within them [2–4]. For example, some macroparasites cause intensity-dependent parasite-induced mortality, and the severity of this process can be reflected in the intensity distribution of parasites across hosts [5,6]. In wildlife–macroparasite systems, such as nematodes, trematodes and ectoparasitic arthropods, the nature of aggregation has been extensively quantified [7,8]: the distribution of macroparasites among hosts is often well-described by a negative binomial distribution, and variance-to-mean relationships are significantly different from Poisson expectations. While we have long been able to quantify the intensity of macroparasites (e.g. by counting parasites following dissection), we can now quantify infection intensity of microparasites by applying modern molecular techniques. Microparasites are organisms such as bacteria, viruses, protozoa and fungi that have high replication rates within a host and often induce host immune responses [9]. While studies on microparasites now regularly report quantitative measures of infection (e.g. viral titres or fungal intensity within a host), we have few baseline expectations regarding what the intensity distributions of microparasites look like and the mechanisms shaping them.

Here, we focus on fungal parasites. Fungal parasites are a global threat to wildlife populations [10]: e.g. *Batrachochytrium dendrobatidis* (Bd), *Batrachochytrium salamandrivorans*, *Ophidiomyces ophiodiicola* and *Pseudogymnoascus destructans* have led to dramatic declines and extinctions in hundreds of wildlife species [11–14]. Like macroparasites, animals infected with fungal parasites suffer intensity-dependent parasite-induced mortality [15,16]. This means that accounting for the distribution of fungal parasite intensity within a population is critical for predicting population-level outcomes following fungal invasion [17,18]. However, despite modelling work increasingly accounting for fungal infection intensity [17,19], we still lack a general understanding of the quantitative patterns of aggregation in host–fungal parasite systems. Quantifying these patterns is important because (i) different levels of aggregation change system dynamics and can significantly affect model predictions [20], and (ii) patterns in fungal intensity distributions may reflect dominant mechanistic processes structuring the host–parasite system [21]. The latter is particularly important for parasites like Bd where cryptic disease-induced mortality may drive ongoing declines [22], but detecting these declines is difficult. Aggregation patterns in fungal intensity distributions could potentially provide a mechanism to detect signatures of disease-induced mortality, as has been done in host–macroparasite systems [6].

Describing the distribution of fungal parasite intensity requires a different statistical and conceptual treatment than traditional macroparasite models. Macroparasite infection intensity is typically described by parasite counts—in other words, how many parasites are found within a host, ranging from zero to some large number. As such, macroparasite counts are discrete and can be described by distributions such as Poisson or negative binomial distribution [8]. By contrast, fungal parasite intensity is typically quantified by molecular approaches such as quantitative PCR (qPCR; [23]). The qPCR technique measures the amount of a specific DNA sequence in a sample by amplifying the sequence while simultaneously detecting and quantifying the fluorescence of the product in real-time as the reaction proceeds. Because the amount of fluorescence generated is directly proportional to the amount of starting DNA, qPCR values correlate with fungal intensity. The resulting measurement of 'infection intensity' is a continuous variable ranging from zero to some arbitrarily large number.

Using infection intensity as a continuous quantity computed by qPCR presents two methodological challenges. First, qPCR measures of infection intensity are subject to substantial measurement error [24,25]. Measurement error can occur when the sample of infection intensity is collected (e.g. the skin of amphibians infected with Bd is swabbed) or when the sample is processed with qPCR [25]). For example, the qPCR process often fails to detect very low quantities of genetic material and can miss low levels of infection [25]. Generally, increasing the noise in a sample owing to measurement error might decrease our ability to detect biological signals. Thus, we might expect measurement error to play a more significant role in affecting the patterns of aggregation in fungal intensity distributions than typical macroparasite distributions, obscuring mechanistic signatures of host–parasite processes on fungal intensity distributions.

Second, discrete distributions that are typically used to describe macroparasite counts are not technically applicable to continuous molecular infection intensity data. In amphibian–Bd systems, there has been some previous discussion on reasonable assumptions for the distribution of infection intensity (particularly with regards to the random component of generalized linear models; [24]) and how approximating a continuous random variable with a discrete random variable (e.g. using a negative binomial distribution to describe infection intensity [24]) can affect the conclusions one draws. However, there has been no systematic examination of the distribution that most consistently describes observed amphibian–Bd distributions or parasitic fungal distributions more broadly. As we continue to develop models for predicting the dynamics of fungal outbreaks, a systematic quantification of the nature of fungal intensity distributions can help direct these modelling efforts, as it has done in traditional macroparasite systems [7,8].

In addition to these statistical differences, there are key biological differences between fungal parasites and macroparasites that may affect observed patterns of aggregation. Fungal parasites grow within/on a host leading to increases in infection intensity. Typically (though not always), macroparasite infections increase in intensity through 'immigration processes' rather than 'birth processes'—hosts accrue parasites through repeated encounters in the environment. Birth processes such as the within-host reproduction of parasites are known to increase the aggregation of macroparasite distributions [26]. An initial expectation might be that fungal distributions are typically more aggregated than macroparasite distributions. However, this prediction is complicated by the speed and mode of transmission of fungal parasites, which can be faster than many macroparasites. For example, Bd can complete its life cycle in 4–10 days, whereas a trematode parasite with multiple intermediate hosts might take months to complete its life cycle [27,28]. This could lead to faster spread, more homogenization and lower levels of aggregation for fungal parasites like Bd compared with macroparasites.

Here, we used 56 912 skin swab samples from 93 amphibian species to ask two main questions: (i) what is the general structure of these Bd fungal intensity distributions, and (ii) do they reflect biological processes? First, we examined whether we see aggregation in host–Bd systems, how these patterns compare with those of macroparasites, and what statistical distribution best describes these fungal intensity distributions. We hypothesized that (i) fungal distributions will be aggregated, (ii) they will show higher levels of aggregation than most macroparasite distributions, and (iii) they will generally conform to a lognormal distribution. Our prediction of a lognormal distribution stems from theoretical work showing that lognormal distributions robustly describe population densities subject to demographic and environmental stochasticity, as well as measurement error [29]. To address our second question, we compared aggregation patterns among amphibian–Bd systems in different epizoological states (e.g. invasion, post-invasion and enzootic) to see if they reflect underlying biological processes. To complement data analysis, we employed an integral projection model to gain insight into the possible mechanisms driving the observed aggregation patterns. Given intensity-dependent disease dynamics in amphibian–Bd systems, we expected reduced aggregation in populations experiencing significant disease-induced mortality, such as those in post-invasion, epizootic states. Similarly, we expected disease-induced mortality to be a critical model parameter in reproducing these patterns.

2. Material and methods

(a) Amphibian–Bd infection intensity data

We analysed four datasets of Bd infection intensities (henceforth 'intensity' or 'load') obtained from amphibian skin swabs collected in the field (see ethics statement for list of permits and approvals for each project). Bd loads were obtained through DNA extraction and qPCR, which detects the number of genomic equivalents or ITS1 copy number of Bd on amphibian skin. These procedures were standardized within but not across datasets. As such, it is important to note that our analysis does not aim to compare absolute values of fungal intensities across datasets or even among disparate sites within datasets. Variations in techniques between laboratories and calculations of Bd intensity (e.g. multiplying by different scaling factors) as well as differences in ITS copy numbers for different strains of Bd in different sites (e.g. [30]), could make comparisons challenging. Instead, we use measures of aggregation (described below) that are scale invariant, thus providing robust measures to analyse aggregation patterns. However, if individuals of the same species of amphibian in the same site in the same season are co-infected with different strains of Bd that vary in their ITS1 copy number (e.g. [31]), then the aggregation metrics we estimate could suffer bias.

The first dataset we included was from Brazil (henceforth the Brazil dataset) which contained 4365 swabs from 41 amphibian species collected primarily within the state of São Paulo (see the electronic supplementary material for details on sampling methods for collection years 2020–2023 and [32] for 2018–2019; and see the electronic supplementary material, figure S1 for general locations of research sites for all datasets). Our second dataset comes from the East Bay region of California (henceforth the East Bay dataset) and contains 10 490 swabs from 11 host species [33]. The third dataset contains 12 457 Bd swabs from amphibians collected from 2016 to 2019 on 43 amphibian species across 31 research sites in four states—Louisiana, Pennsylvania, Tennessee and Vermont [34]. Although collected across a wide geographical range, swabs from this study were all processed at a centralized location using a consistent methodology. Therefore, we will refer to this dataset broadly as the eastern US dataset. Our final dataset is from the Sierra Nevada mountains of California (henceforth the Sierra dataset) and contains 29 600 samples collected from mountain yellow-legged frogs (MYL frogs; composed of sister species *Rana muscosa* and *Rana sierrae*) at high elevation lakes, ponds and wetlands [15,17].

Samples within each dataset were grouped based on host species, life stage (larva (i.e. tadpole in anuran species), subadult or adult), research site, season (Brazil: wet or dry; East Bay and Sierra: summer; eastern US: winter, spring, summer or autumn) and year (see the electronic supplementary material, table S1 for more detailed composition of each dataset). Moving forward, we will refer to a particular combination of species, life stage, research site, season and year as a 'group'. Examining specific 'groups' allows us to quantify the patterns of Bd aggregation in a biologically relevant temporal period at a particular location. In total, the Brazil dataset had 109 candidate groups for analysis, East Bay had 714, eastern US had 391 and the Sierra had 647.

(b) Question 1a: are fungal intensity distributions aggregated and how do these compare with aggregation patterns in macroparasite systems?

To address this question, we analysed aggregation in the fungal intensity distributions using Taylor's Power Law (TPL) which relates the log mean and log variance in fungal intensity, calculated for each group. This metric allows for direct comparison to the macroparasite literature. Specifically, we focused on the slope of TPL as a metric of aggregation, where a greater slope indicates greater aggregation [3,26]. Across all datasets, we only included groups with at least three infected individuals, yielding 961 groups across all four datasets (electronic supplementary material, table S1).

We first fitted a linear regression to the log mean versus log variance relationship for each of the four datasets and calculated the slope. We compared the slopes with the empirical relationship previously seen in many macroparasite populations (slope = 1.55, 95% confidence interval (CI): [1.48,1.62]) [7]. Notably, this slope represents the trend for many but not all macroparasite systems [21,26], and because fewer studies have examined microparasite aggregation (but see [35,36])—particularly on a large scale—we did not compare Bd patterns with those of other microparasites. Nonetheless, we explored their relationship to a Poisson distribution (mean-variance slope equal to 1), which is generally considered the null distribution in many host–macroparasite studies [2]. However, the continuous nature of Bd load data also suggests considering the alternative null with a TPL slope of 2. A baseline

of TPL slope of 2 has been used to describe the aggregation of free-living organisms in space and time [37,38]. Moreover, given our expectation of a lognormal distribution of Bd intensity across hosts, we would expect a TPL slope of 2 based on the simple definitions of the mean and variance for a lognormal distribution. Note that for this analysis, the log mean and the log variance for each group were computed using both infected and uninfected individuals, consistent with macroparasite studies.

Second, to explore variability in the slope of TPL across the 36 species with sufficient sampling, we ran a linear mixed effect model (i.e. Gaussian error) with random effects of amphibian species and subregion on the intercept and slope. Specifically, the model we fitted was log(variance) ~ log(mean) + (1 + log(mean)|subregion) + (1 + log(mean)|species), where subregion was a factor with the following levels: East Bay, Sierra, Pennsylvania, Tennessee, Vermont, Louisiana and Brazil. We then examined the species-specific TPL slopes and compared them with the macroparasite slope from Shaw & Dobson [7], the *Gyrodactylus* slope from Lester & McVinish [21] and the *Oxyuridae* slope from Grear & Hudson [26].

(c) Question 1b: what distribution best describes fungal intensity distributions?

To characterize the shape of fungal intensity distributions conditional on infection, we considered continuous distributions of non-negative real numbers: gamma, exponential, lognormal and Weibull. We did not consider Poisson and negative binomial distributions because fungal intensity, as assessed using qPCR, is a continuous measure. Although qPCR results can be transformed into integer values and analysed using standard generalized linear models [39], we opted to keep the data on the continuous scale, consistent with previous models [19]. Each of the continuous distributions can capture a strong right skew in intensity distributions, consistent with canonical patterns in host–macroparasite systems. The gamma distribution is the continuous analogue to the negative binomial distribution, a distribution that describes many macroparasite populations [8]. Similarly, the exponential is a special case of the gamma distribution that is represented by only one parameter and is analogous to the discrete geometric distribution which has been proposed as a potential null distribution in host–macroparasite systems [40,41]. Lognormal distributions are found throughout natural systems empirically and theoretically [29] and are representative of non-negative metrics with relatively low means but large variance. Finally, we considered the Weibull distribution, which is typically used to model 'time-to-failure' or survival analyses but has been used to describe macroparasite aggregation data [42].

For this analysis, we only considered groups with at least 10 infected individuals to ensure we had power to distinguish between competing distributions. This resulted in 525 groups. We used the fitdistrplus package in R to fit exponential, lognormal, Weibull and gamma distributions using maximum-likelihood estimation (MLE) or moment-matching estimation, if the MLE model would not converge. We compared Akaike information criterion (AIC) values across distributions to find the best predictive model, assuming no notable difference in performance when AIC values were within ±2.

(d) Question 2: do patterns of aggregation in Bd intensity reflect biological processes, such that there are quantifiable differences in aggregation between epizoological states?

To address this question, we used a metric that can be applied to a single group (unlike TPL) known as Poulin's discrepancy index, or simply Poulin's D [4,43]. Poulin's D is bounded from 0 to 1 and is a proportional measure of the difference between an observed distribution and a uniform distribution. A higher value indicates greater discrepancy from a uniform distribution and is suggestive of higher aggregation. The equation for Poulin's D is $D = (\sum_{i=1}^{n} \sum_{j=1}^{n} |x_i - x_j|)/(2n^2\bar{x})$, where x is the fungal load of host i or j, n is the total number of hosts and $\bar{x} = \sum_{i=1}^{n} x_i/n$ (we use the equation given in [44], which is the Gini index). We also calculated the coefficient of variation (CV) on the natural scale and other related metrics—$\log_{10}$-transformed CV on the natural scale and CV on the $\log_{10}$ scale—which should provide comparable results to Poulin's D [44]. We calculated CV on the $\log_{10}$-transformed data to determine if trends remained similar on different scales. When calculating our aggregation metrics, we excluded uninfected individuals to remove the effect of prevalence on the observed patterns. We only included groups that had at least two infected individuals—the minimum number for a meaningful value of our metrics. We also explored only including groups with a minimum of 10 infected individuals, and our results were unchanged.

For this question, we focused on the Sierra dataset. Of the datasets used in this study, the Sierra dataset is unique because, for many southern populations in the Sierra Nevada, we know when Bd invaded, when epizootics ensued and when populations declined [15,34]. Moreover, for more northern populations, such as those in Yosemite National Park, we know that populations are past the invasion–epizootic–declining phase and are persisting enzootically with Bd [17,45]. Thus, we have three clearly definable epizoological phases for MYL–Bd populations in the Sierra Nevada: (i) invasion stage (when Bd prevalence is less than 50% in a population; [46]) (ii) post-invasion phase (consisting of epizootic host declines or recent declines), and (iii) enzootic phase (Bd invaded before the early 2000s and amphibian populations are persisting in the presence of Bd). Moreover, from targeted field surveys and laboratory experiments, we know that there is strong intensity-dependent mortality in MYL frogs [15,19]. If patterns of Bd aggregation contain information about intensity-dependent mortality, we would expect a notable reduction in Bd aggregation for higher mean infection intensity in MYL frog populations [3]. In other words, mortality in highly infected individuals would effectively reduce the tail of the right-skewed distribution characteristic of aggregated populations, thereby decreasing aggregation.

To explore signatures of epizoological phase on Bd aggregation, we first plotted each metric—Poulin's D, CV, log CV and CV of log-scale data—against mean $\log_{10}$-transformed Bd intensity and asked whether populations in known epizoological phases clustered in mean intensity-aggregation space (henceforth intensity-aggregation space) and whether there were notable reductions in aggregation at high infection intensities (note that epizoological phases were determined independently of aggregation

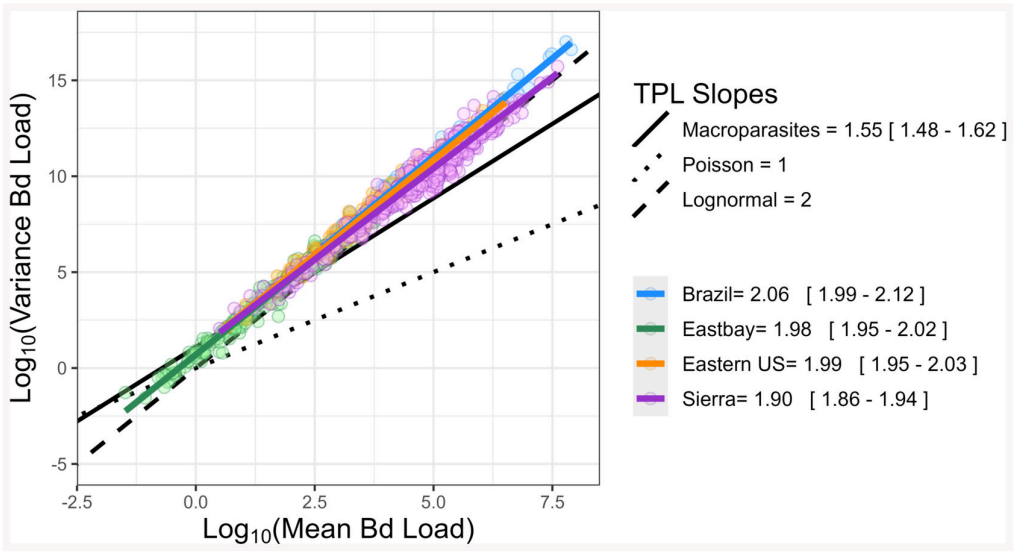

Figure 1. The relationship of log mean and log variance fungal intensity for all groups. Regression lines were fitted to each dataset (slopes and 95% CIs in legend). For reference, the slope is typically seen in macroparasites (1.55, 95% CI [1.48–1.62]) [7] (solid black), a slope of 1 expected in a Poisson—or macroparasite null—distribution (dotted) and a slope of 2 expected for a lognormal distribution (dashed) are provided.

or mean infection intensity). We used beta regression [4] to test for a quadratic effect of mean infection intensity on aggregation metrics, where a strong quadratic effect is indicative of aggregation being reduced at high infection intensity.

Finally, to better understand how mechanisms such as intensity-dependent mortality and epizoological phase could theoretically affect patterns of aggregation in host–fungal systems, we adapted an integral projection model (IPM) that has been previously developed for amphibian–Bd systems [19]. In short, IPMs provide an approach for modelling intensity-dependent infection dynamics of host–fungal interactions by specifically modelling the entire distribution of fungal intensities within a population (see the electronic supplementary material for more detail). Hosts are born uninfected, and in the absence of disease, the host population grows logistically towards a carrying capacity. In one time step of the model, hosts may become infected by encounters with environmental pathogens and gain some initial log number of parasites (infection load). Parasites grow within hosts, with some stochasticity, towards a within-host carrying capacity. In each time step, infected hosts have a probability of recovery from infection and a probability of survival, both of which decline with infection load. Infected hosts shed parasites back into the environment proportional to the number of parasites they currently hold. We simulated disease invasion for 1 year to represent the effects of disease spread without host evolution. We then added simulations where we included multiple host genotypes with different traits to simulate evolution over 30 years (a relevant timescale for the MYL–Bd system). Specifically, we focused on host evolution of resistance that lowers pathogen growth rate, an important mechanism in the MYL–Bd system [39,45]. We performed simulations at parameter values from laboratory experiments for the MYL–Bd system (see the electronic supplementary material, table S2) and then explored how varying certain parameters impacted the intensity-aggregation patterns in our simulations. We calculated the same four aggregation metrics in our simulations as were calculated from field data to determine intensity-aggregation patterns. We did this to investigate the patterns that could emerge in intensity-aggregation space for the different metrics and if they are indicative of specific biological mechanisms.

3. Results

(a) Question 1a: are fungal intensity distributions aggregated and how do these compare with aggregation patterns in macroparasite systems?

Based on TPL, Bd showed a greater degree of aggregation compared with the macroparasites presented by Shaw and Dobson (slope: 1.55, 95% CI [1.48–1.62]) [7]. The slopes of TPL across the groups for each dataset ranged between 1.90, 95% CI [1.86–1.94] (Sierra) and 2.06, 95% CI [1.99–2.12] (Brazil) (figure 1). Therefore, the variance of Bd infection intensity increases to a greater degree with respect to average fungal load than many macroparasites. However, some macroparasites have comparable or notably higher slopes than what we found in Bd (e.g. *Gyrodactylus* spp. 2.08, 95% CI [1.66–2.44] [21]; *Oxyuridae* spp. 2.80, 95% CI [2.40–3.20] [26]).

We examined how the slopes of TPL varied among amphibian species, host life stages and epizoological phase. We found that including slope as a random effect among host species yielded a better predictive model than a model without this effect (ΔAIC = 13.6). Though these slopes vary enough to impact the model's predictive capabilities, they are relatively clustered and all more aggregated than the macroparasites presented by Shaw and Dobson (see the electronic supplementary material, figure S2) [7]. These slopes fell within the 95% CI for *Gyrodactylus* macroparasite species [21] and are significantly lower than the slopes seen in

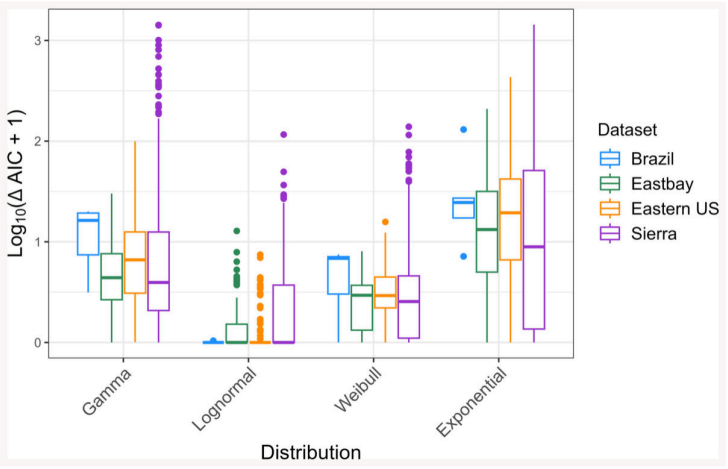

Figure 2. Comparison of $\log_{10}(\Delta AIC + 1)$ values across four continuous distributions that were fitted to 525 amphibian groups' fungal intensity data across four datasets. Each data point is a host group with at least 10 infected individuals.

Oxyuridae [26]. We found a similar pattern across host life stage, showing slopes greater than that of Shaw and Dobson's macroparasite slope. However, the slopes for each life stage were statistically distinct: larval (1.85, 95% CI [1.82–1.89]), subadult (1.93, 95% CI [1.91–1.95]) and adult (2.03, 95% CI [2.00–2.05]). We also applied these analyses to the Sierra dataset and compared across epizoological phases. We found that the slope for populations considered to be enzootic was statistically steeper (i.e. more aggregated; 2.08 95% CI [2.00–2.16]) than those in a post-invasion epizootic state (1.92 95% CI [1.86–1.99]) (see the electronic supplementary material, figure S3).

(b) Question 1b: what distribution best describes fungal intensity distributions?

Of the distributions that we fitted to the Bd-positive data, the lognormal model consistently performed better than the others, as determined by comparing AIC scores (figure 2). Assuming models perform equally well if AIC scores are within 2 units of each other, over half of the groups (57.3%) were well-described by multiple distributions. The lognormal performed best or just as well as another model in 76.7% of the groups, the Weibull in 58.8%, the gamma in 35.2% and the exponential in 25.7%. The lognormal model also fitted 38.0% of groups better (>2 AIC units) than any of the other models, whereas the Weibull, gamma and exponential models performed better than all others in 4.4%, 0.4% and 0% of the groups, respectively.

With the lognormal model outperforming the other distributions, we sought to determine if the lognormal is objectively a good fit to the data. We used a Shapiro–Wilk's test of normality on the log-transformed data, after adjusting the *p*-values for multiple tests to account for false-discovery rate (using the p.adjust function in R with method fdr). For 96.7% of sampled groups, we fail to reject the null hypothesis that the data follow a normal distribution (electronic supplementary material, figure S4, at an adjusted significance level of $\alpha = 0.05$). Cognizant that failure to reject the null is not proof of the null, we conclude there is no strong evidence that distributions deviate from a lognormal distribution.

(c) Question 2: do patterns of aggregation in Bd intensity reflect biological processes, such that there are quantifiable differences in aggregation between epizoological states?

(i) Empirical results

To gain mechanistic intuition on the broader results in this section, we first examined seven specific populations from the Sierra dataset that (i) were repeatedly surveyed during Bd invasion and declines, and (ii) had sufficient samples of infected adults or subadults at a minimum of three time points to compute Poulin's *D* ($n \geq 2$). Figure 3A shows the abundance trajectory of adult frogs in these populations through time, including the well-known pattern of dramatic population declines following Bd invasion. In figure 3B, we plot these same populations in intensity-aggregation space and see a consistent counterclockwise pattern emerge. Upon invasion, mean infection intensity is low, and aggregation is low. Once the population transitions to the post-invasion phase, mean intensity is high, but aggregation remains relatively low. As the population progresses through the epizootic, mean intensity declines and aggregation increases. These patterns suggest that there is a signature of epizoological phase on observed patterns of aggregation.

To examine this pattern more broadly, we plotted 313 Sierra groups in intensity-aggregation space and observed a strong clustering of invasion, post-invasion and enzootic groups (figure 4A–D) that was consistent with what we saw in our seven focal populations with time-series data (figure 3B). Namely, the invasion stage was characterized by low mean intensity and low aggregation, the post-invasion phase was characterized by medium to high intensity and high to low aggregation and the enzootic phase was characterized by intermediate mean intensity and high aggregation. These groupings of phases in intensity-aggregation

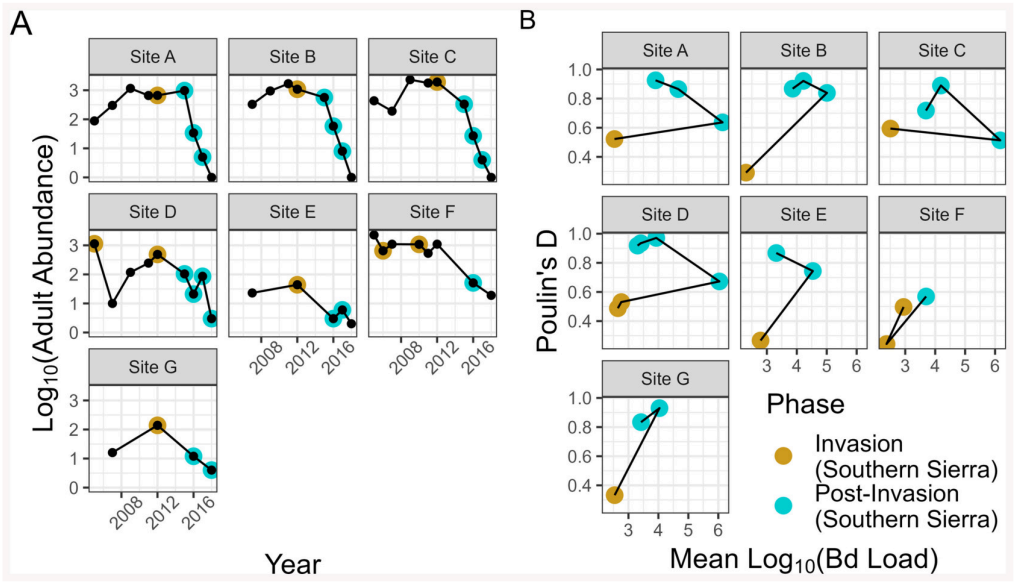

Figure 3. (A) The adult abundance trajectories of seven focal MYL frog populations through time. Black points show each time the population was surveyed and coloured points indicate when a sufficient number of infected individuals ($n \geq 2$) were sampled to compute Poulin's *D*, with a higher value indicating more aggregation. The invasion phase was delineated when prevalence was less than 0.5 [46]. (B) The same seven populations with trajectories plotted in intensity-aggregation space. The coloured dots in (B) correspond to those in (A).

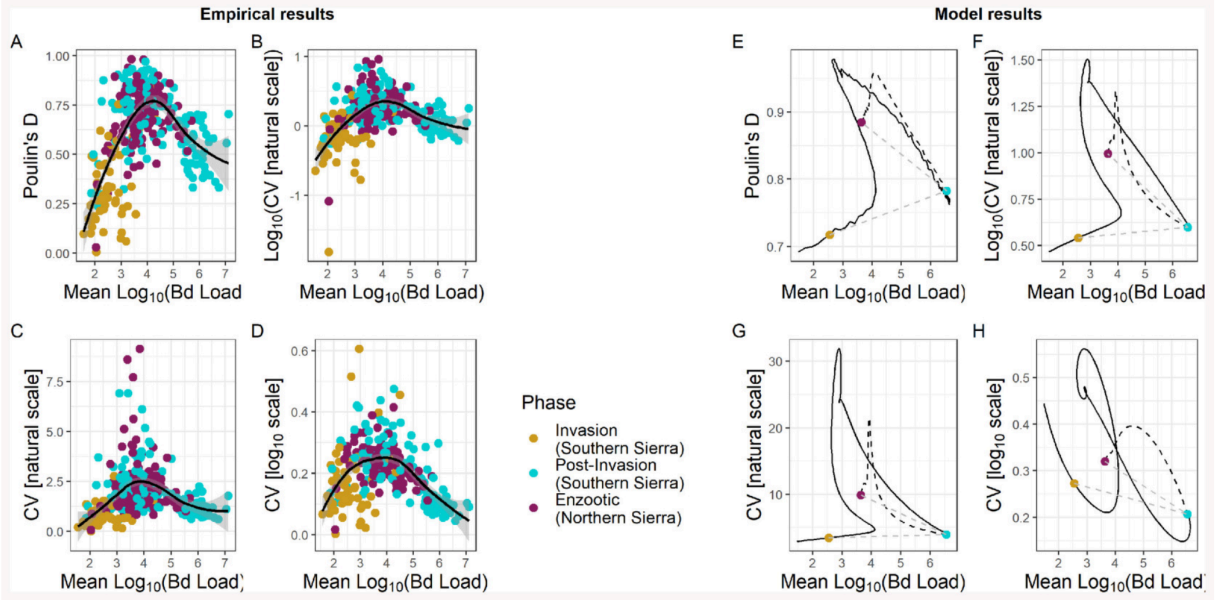

Figure 4. Groups in different epizoological phases plotted as a relationship between mean $\log_{10}$ Bd intensity and different aggregation metrics. (A) Soon after Bd invasion, mean loads and aggregation (Poulin's D) are low (yellow points). Later, post-invasion, mean loads are high and aggregation is still relatively low (blue points). Then much later, mean loads are intermediate and aggregation is higher (purple points), leading to an overall unimodal shape. This same pattern holds for other aggregation metrics including (B) $\log_{10}$ of CV (coefficient of variation) on the natural scale, (C) CV on the natural scale and (D) CV on the $\log_{10}$ scale. The unimodal trend for all empirical results is emphasized through a best-fit spline (black, 95% CI shaded grey). A parameterized IPM model can generally reproduce these hump-shaped patterns in all four metrics without evolution (black curve in (E–H)); we compare across each metric as the model need not necessarily produce a hump shape in every metric (see the electronic supplementary material, figures S6 and S7). Evolution of lower pathogen growth rate (dashed black) moves populations to lower mean loads and higher aggregation metrics, generally matching the empirical results for enzootic populations. We plot the points corresponding to sampling the model results at one week (invasion, yellow), 1 year (post-invasion, blue) and 31 years (enzootic, purple) for comparison with the empirical results in figure 3B; low temporal resolution sampling can create a counterclockwise pattern in intensity-aggregation space (emphasized by dotted grey line connecting coloured points in (E–H).

space align with the differences seen between enzootic and post-invasion populations based on TPL analyses (see the electronic supplementary material, figure S3).

A distinct pattern that emerges in figure 4A–D is the notable unimodal shape of the data in intensity-aggregation space. The downward curvature is consistent with predictions from host–macroparasite theory that intensity-dependent mortality should reduce aggregation for high mean intensities as it truncates the tail of the Bd intensity distribution, resulting in lower variance for

a given mean within a population. This pattern was statistically supported by a strong quadratic effect of mean intensity on aggregation, with the quadratic model performing better than the linear effect-only model (ΔAIC = 150.13 from comparing a model with quadratic effect to one with only a linear relationship). Moreover, this unimodal pattern was robust to different measures of aggregation (figure 4A–D).

Interestingly, putative enzootic populations rarely occupy the space of high mean intensity and low aggregation (figure 4). We observed seven enzootic populations in this region of high mean intensity and lower aggregation. Although one group in the enzootic stage was composed of adults, the rest were subadults—a life stage that still experiences substantial disease-induced mortality even in enzootic populations [45].

(ii) Modelling results

Modelling showed that the unimodal intensity-aggregation patterns probably contain important, mechanistic information about disease processes. The hump-shaped patterns in intensity-aggregation space found in the field data for all four metrics did not emerge trivially from the model; depending on parameter values, the model simulations produced this hump shape for none, some or all metrics. Simulations with parameter values based mostly on laboratory experiments [19] did not produce unimodal patterns for any of the four metrics (electronic supplementary material, figure S6), indicating different biological processes may occur in the field than in a laboratory setting. This possibility of a quantitative mismatch between the laboratory and the field is also supported by the observation that the laboratory-based parameter values produced significantly lower values of intensity and higher values of aggregation than were observed in the field. To address this possible mismatch, we explored additional parameter sets (details in the electronic supplementary material). When we weakened the negative density dependence of pathogen growth within hosts and decreased the variance in initial infection load, our simulations produced slightly higher mean loads, lower aggregation and a unimodal pattern in one metric, matching the field data somewhat better (electronic supplementary material, figure S7). When we also decreased host mortality, parasite shedding rate (keeping prevalence from maxing out at one) and stochasticity in parasite growth, the model simulations produced higher intensities and still lower aggregation. Moreover, the model produced unimodal patterns for all four metrics (figure 4E–H). Thus, in terms of matching the intensity-aggregation patterns from the field, we considered this our best parameter set.

From host–macroparasite theory, we might expect that this unimodal pattern depends on intensity-dependent mortality driving lower aggregation at high intensity. Changing the parameter values so that hosts could survive very high loads with no mortality did increase aggregation somewhat, as expected, but unexpectedly did not significantly change the unimodal patterns (electronic supplementary material, figure S9). Finally, the path our simulation results take through intensity-aggregation space may explain observed counterclockwise motion through intensity-aggregation space for populations in figure 3B; if we sample our simulated populations at one month, 1 year and 30 years to simulate the infrequent sampling of the field populations, we see how a counterclockwise motion could arise (e.g. coloured points in figure 4E–H).

Our modelling further shows that the position of the enzootic populations in intensity-aggregation space may be a signal of host evolution. Host evolution of resistance that lowers pathogen growth rate moves populations left, towards lower mean intensity and up, towards higher aggregation, in intensity-aggregation space for all four metrics (dashed black in figure 4E–H). This position of post-evolution populations higher and to the left of post-invasion populations that have experienced an epizootic but not yet evolved is consistent with the field data (figure 4). If hosts evolved a different defence, e.g. tolerance of higher parasite loads without dying, we would not observe this shift (electronic supplementary material, figure S8). Thus, the enzootic populations' position in intensity-aggregation space may indicate the evolution of resistance rather than tolerance in the host.

4. Discussion

Parasite aggregation is a strong driver of disease dynamics within host populations [20]. Though aggregation in macroparasites has been extensively examined, it has not been systematically explored within host–fungal parasite systems, despite the known impact of fungal pathogen intensity on its host. In this study, we used a dataset of nearly 57 000 samples of amphibian infection intensity to show that (i) Bd is consistently more aggregated than typical macroparasites, (ii) the distribution of Bd intensity within a population is generally consistent with a lognormal distribution, and (iii) patterns of Bd aggregation can contain consistent signatures of biological mechanisms. This study demonstrates the use of fungal aggregation as a means of identifying cryptic biological processes (e.g. disease-induced mortality or evolution of defence mechanisms) within host populations that could be applied to other host–fungal systems.

(a) Patterns of aggregation

Both macroparasites and Bd are aggregated within hosts, and we expect this pattern to hold in other fungal systems as well. However, the relative degree of aggregation may vary based on host and parasite. For Bd, we found high consistency in aggregation levels that were generally significantly greater than those of many macroparasite systems, with some notable exceptions. For instance, *Gyrodactylus* [21] flatworms and *Oxyuridae* pinworms [26] rapidly reproduce within their hosts and tend to aggregate in levels akin to or greater than Bd TPL slopes (2.08 [1.66, 2.49] and 2.82 [2.44, 3.22], respectively). This would support the hypothesis that fungal aggregation levels are driven—at least in part—by the parasite's ability to reproduce on its original host. That is, already-infected hosts can acquire additional infection faster than uninfected hosts, increasing the variance and skew in the distribution of parasites. However, a second explanation for these TPL patterns may exist; namely, these attributes may be a

product of statistical constraints that are independent of parasite biology (e.g. [3,41]). This has been suggested for macroparasites as well to explain the highly conserved nature of aggregation across systems, despite the widely varying biology. We see similar consistency in our Bd systems across host species and sites. Given that these systems tend to follow a lognormal distribution, we would expect a TPL slope of 2, which is generally consistent with what we observe across Bd systems. Lognormal distributions describe the spatial distribution of abundance and density of organisms in many natural systems and theoretically emerge in populations experiencing environmental and demographic stochasticity [29]. It is possible that the lognormal distribution of Bd (and thus the TPL slope of 2) arises because Bd dynamics, swabbing and testing are a combination of multiplicative random processes that necessarily lead to a lognormal distribution (i.e. a central limit theorem type of argument [47]). Regardless of the exact drivers, we found that Bd aggregation does not look like that of many macroparasites.

The fit of the lognormal distribution to the Bd data—conditional on infection—was similar across species, life stages and locations. This has important modelling implications, as fitting empirical data to models generally requires making some distributional assumptions about fungal intensity. Currently, host–fungal models in amphibian–Bd systems have assumed that Bd intensities are approximately lognormally distributed [34,48], but this assumption has only been validated for a few focal amphibian–Bd systems. Our results show that a lognormal assumption is broadly applicable within amphibian–Bd systems, making theoretical and applied applications of these models robust across amphibian–Bd systems. While we only examined Bd in this study, we expect approximate lognormal distributions to hold more broadly across host–fungal systems. Testing this expectation is an important next step for uniting host–fungal dynamics under a common theoretical framework, as has been so successfully done with host–macroparasite dynamics.

(b) Mechanisms of aggregation

While Bd aggregation was highly consistent across amphibian species and populations, we found that there are also distinct patterns that arise in fungal aggregation that reflect underlying biological processes. In the empirical data, we observed a notable reduction in aggregation in post-invasion populations that we know were experiencing high levels of disease-induced mortality (based on previous field observations, [15]). Moreover, we observed that the life stage in enzootic populations with the lowest levels of aggregation tended to be juveniles, the life stage in which disease-induced mortality is still occurring at a high rate even in enzootic populations [39]. While it is tempting to conclude that this pattern of reduced aggregation is solely driven by intensity-dependent mortality as predicted in host–macroparasite systems [2,3], our modelling results show that reduced aggregation in post-invasion populations can arise even in the absence of intensity-dependent mortality.

The mechanism by which our model can produce the observed unimodal pattern in intensity-aggregation space is described as follows. When Bd first invades a population, the observed intensity distribution is primarily structured by the dynamics of initial infection so that hosts have relatively similar low loads and low levels of aggregation. As the Bd outbreak proceeds, the distribution of fungal intensity begins to include both older infections with higher loads structured by within-host growth dynamics and newer infections with loads structured by initial infection dynamics. This mixture of newer and older infections increases aggregation in the intensity distribution. Most hosts become infected as the outbreak continues, and most infections are older and closer to the pathogen's within-host carrying capacity. This drives a subsequent increase in mean intensity and reduction in aggregation. Overall, the shift from mostly newer infections to a mixture of newer and older infections then finally to mostly older infections drive a unimodal pattern in intensity-aggregation space. Our model shows that while we can get the expected unimodal pattern of reduced aggregation being driven predominantly by intensity-dependent mortality, the pattern requires that (i) all hosts get infected essentially simultaneously, and (ii) hosts rarely lose infection during an outbreak. However, as these conditions are violated, the effect of intensity-dependent mortality on aggregation quickly becomes dwarfed by the joint effect of initial infection and within-host growth. Host–macroparasite theory has shown that there is not always a one-to-one mapping between aggregation patterns and biological processes [49]. Our results clearly highlight this point for fungal intensity distributions—there are two plausible biological mechanisms that could explain and jointly contribute to the observed reduction in aggregation at high loads: intensity-dependent mortality and the balance between initial infection and within-host growth along an epizoological trajectory. The latter is an aggregation mechanism that, to our knowledge, has not been considered in macroparasite systems, highlighting the need for unique theory describing the patterns and mechanisms of aggregation in host–fungus systems.

In addition to intensity-dependent mortality and the balance between initial infection and within-host growth, we found that patterns of aggregation contained clear signatures of the epizoological stage of a host–Bd system. Empirically, we saw populations follow a characteristic counterclockwise pattern on the yearly time scale in intensity-aggregation space. Interestingly, our modelling results illustrated that this counterclockwise pattern was probably a result of the timescale on which we observed these MYL frog–Bd systems. Our model showed that the transition from invasion phase to post-invasion epizootic phase should actually traverse a humped curve, rather than seamlessly jumping from the left to the right side of the curve. Because these sites were only sampled once a year, these data probably missed the transition from invasion phase (< 50% prevalence) to post-invasion phase (> 50% prevalence), as this often occurs rapidly within MYL frog–Bd systems. Therefore, we could only observe the invasion point and the post-invasion epizootic point within the intensity-aggregation space. Moreover, our model shows that the transition back to an intermediate intensity and high aggregation state does not occur in the model without some level of evolution in host defence; specifically, host evolution of resistance that lowers pathogen growth rate produced this pattern, while evolution of tolerance could not. MYL frog populations have persisted enzootically and begun to recover, probably owing to evolved resistance to Bd [39]. As such, this is an intriguing basis for using population-level aggregation patterns to identify biologically relevant processes in wild populations, such as the evolution of host defence.

Examining aggregation patterns in a system where epizoological phase was known *a priori* enabled us to discern patterns across the intensity-aggregation space. The full epizoological trajectory of many amphibian populations is rarely observed, and it is well known that similar amphibian populations infected with Bd can be at different places along an epizoological trajectory or on different trajectories altogether [50]. By substituting spatial replication across populations for temporal replication within populations, we show that intensity-aggregation space can help locate disparate populations along a common epizoological trajectory. We expect the approach we develop to be particularly useful for species that are generally considered to be persisting enzootically with Bd, but in reality, may be experiencing cryptic invasions and epizootics across populations (e.g. electronic supplementary material, figure S5). Such use of aggregation patterns could be used in other host–fungal systems, such as white-nose syndrome and snake fungal disease, and may be pivotal in our future analyses and understanding of these systems.

5. Conclusions

Beyond amphibian–Bd systems, our study is useful for understanding fungal parasite dynamics in other wildlife populations. By extending our analyses to other host–fungal parasite systems, such as white-nose syndrome in bats, *B. salamandrivorans* in amphibians, snake fungal disease or those of public health concern like aspergillosis and blastomycosis, we can elucidate broader patterns of aggregation of fungal parasites. This comparative approach can unveil commonalities and distinctions in fungal intensity patterns across different hosts and parasites. Identifying patterns of aggregation and how they reflect biological processes in diverse systems has implications for conservation strategies, disease management and disease modelling efforts. By demonstrating the ubiquity of aggregation, identifying distributional characteristics and deciphering the biological significance of these patterns, we advance our understanding of host–fungal parasite ecology and pave the way for broader consideration of the implications of microparasite aggregation in wildlife disease ecology and epidemiological theory.

Ethics. Animal use in this research was approved and overseen by the following institutions: University of Pittsburgh (IACUC Protocol no.1602771); Vanderbilt University (IACUC no.M16002500); UMass (IACUC no.2014003); São Paulo Research Foundation (FAPESP propc no.2021/10639-5); Brazilian National Council for Scientific and Technological Development (CNPq proc no.304713/2023-6); São Paulo State University - UNESP (Protocol no.0597-1 & no.0597-2); Federal University of São Carlos (Protocol no.2464230518); Brazilian Government (Sisbio no.74576, no.63917 and Sisgen no.A663126, no.AC2F7B2, no.AC88222, no.AE285E3); Fundação Florestal do Estado de São Paulo (FF no.260108-005.880/2018, no.003838/2020-26); UA IACUC no.20-05-3622; Pennsylvania State University (IACUC no.PROTO202102112); University of California-Santa Barbara; Sierra Nevada Aquatic Research Laboratory. Other support came from the following: East Bay Regional Parks and Municipal Utility Districts; Santa Clara County Parks; Sequoia-Kings Canyon and Yosemite National Parks; Inyo and Sierra National Forests; Louisiana Department of Wildlife and Fisheries (Scientific Research and Collecting Permits LNHP-17-029, LNHP-18-005, WDP-19-010); Pennsylvania Fish and Boat Commission (Permit 2018-01-0360); Tennessee Wildlife Resource Agency (Scientific Collection Permit no.1546); Vermont Fish and Wildlife Department (Permit SR-2016-17); California Department of Fish and Wildlife; U.S. Fish and Wildlife Service; and multiple private landowners.

Data accessibility. Data are available from the Dryad Digital Repository: [51]. Data supporting this research is provided from the following publications: [15,17,32–34].

Supplementary material is available online [52].

Declaration of AI use. We have not used AI-assisted technologies in creating this article.

Authors' contributions. S.A.R.S.: conceptualization, formal analysis, methodology, validation, visualization, writing—original draft, writing—review and editing; J.C.W.: conceptualization, formal analysis, methodology, validation, visualization, writing—original draft, writing—review and editing; J.DeM.: conceptualization, formal analysis, writing—review and editing; E.H.LeS.: data curation, investigation, writing—review and editing; M.E.B.O.: data curation, investigation, writing—review and editing; L.A.R.-S.: data curation, funding acquisition, investigation, writing—review and editing; C.J.B.: data curation, funding acquisition, investigation, writing—review and editing; C.L.R.-Z.: data curation, funding acquisition, investigation, writing—review and editing; D.C.W.: data curation, funding acquisition, investigation, writing—review and editing; R.A.K.: data curation, funding acquisition, investigation, writing—review and editing; T.C.S.: data curation, funding acquisition, investigation, writing—review and editing; C.F.B.H.: investigation, writing—review and editing; C.G.B.: data curation, funding acquisition, investigation, writing—review and editing; P.T.J.J.: funding acquisition, investigation, writing—review and editing; M.Q.W.: conceptualization, data curation, formal analysis, funding acquisition, methodology, project administration, supervision, validation, visualization, writing—original draft, writing—review and editing.

All authors gave final approval for publication and agreed to be held accountable for the work performed therein.

Conflict of interest declaration. We declare we have no competing interests.

Funding. This project was supported by the National Park Service (to R.A.K.), Yosemite Conservancy (to R.A.K.), the US Fish and Wildlife Services Endangered Species Conservation and Recovery Grant Program, the National 503 Science Foundation (EF-0723563, to C.J.B.; DEB-1557190, to C.J.B.; DEB-2133401, to M.Q.W.; and DBI-2120084, to C.L.R.Z., DBI-2120084, to RIBBiTR; DEB-2227340, to C.G.B.; IOS 2303908, to C.G.B.; BII-2120084, to C.G.B.; DEB-2133401, to M.Q.W; DEB-2133399, to T.C.S; DEB-1149308; DEB-1754171), and the NIH/NSF Ecology and Evolution of Infectious Diseases program (R01GM109499 and R01GM135935).

Acknowledgements. We thank T. McDevitt-Galles, W. Moss, D. Calhoun, R. Chen, T. Riepe, K. Leslie, A. Barbella, K. Rose, Dan Wetzel, Aimee Danly, Caitlin Nordheim, Miranda Kosowsky, Laura A. Brannelly, Karie A. Altman, Renato A. Martins, J. Vargas Soto, E. Hegeman and A. Lindauer, Carolina Lambertini, Shannon Buttimer, Wesley Neely, Daniel Medina, Jack Boyette and the many other individuals who helped with data collection, processing, management and conceptual insights.

References

1. Poulin R. 2007 Are there general laws in parasite ecology? *Parasitology* **134**, 763–776. (doi:10.1017/s0031182006002150)
2. Anderson RM, Gordon DM. 1982 Processes influencing the distribution of parasite numbers within host populations with special emphasis on parasite-induced host mortalities. *Parasitology* **85**, 373–398. (doi:10.1017/s0031182000055347)
3. Johnson PTJ, Wilber MQ. 2017 Biological and statistical processes jointly drive population aggregation: using host-parasite interactions to understand Taylor's power law. *Proc. R. Soc. B* **284**, 20171388. (doi:10.1098/rspb.2017.1388)

4. Morrill A, Nielsen ÓK, Skírnisson K, Forbes MR. 2022 Identifying sources of variation in parasite aggregation. *PeerJ* **10**, e13763. (doi:10.7717/peerj.13763)
5. Lester RJG. 1984 A review of methods for estimating mortality due to parasites in wild fish populations. *Helgoländer Meeresuntersuchungen* **37**, 53–64. (doi:10.1007/bf01989295)
6. Wilber MQ, Briggs CJ, Johnson PTJ. 2020 Disease's hidden death toll: using parasite aggregation patterns to quantify landscape-level host mortality in a wildlife system. *J. Anim. Ecol*. **89**, 2876–2887. (doi:10.1111/1365-2656.13343)
7. Shaw DJ, Dobson AP. 1995 Patterns of macroparasite abundance and aggregation in wildlife populations: a quantitative review. *Parasitology* **111**, S111–S133. (doi:10.1017/s0031182000075855)
8. Shaw DJ, Grenfell BT, Dobson AP. 1998 Patterns of macroparasite aggregation in wildlife host populations. *Parasitology* **117**, 597–610. (doi:10.1017/s0031182098003448)
9. Anderson RM, May RM. 1979 Population biology of infectious diseases: part I. *Nature* **280**, 361–367. (doi:10.1038/280361a0)
10. Fisher MC, Henk DA, Briggs CJ, Brownstein JS, Madoff LC, McCraw SL, Gurr SJ. 2012 Emerging fungal threats to animal, plant and ecosystem health. *Nature* **484**, 186–194. (doi:10.1038/nature10947)
11. Langwig KE, Hoyt JR, Parise KL, Kath J, Kirk D, Frick WF, Foster JT, Kilpatrick AM. 2015 Invasion dynamics of white-nose syndrome fungus, Midwestern United States, 2012–2014. *Emerg. Infect. Dis*. **21**, 1023–1026. (doi:10.3201/eid2106.150123)
12. Lorch JM *et al*. 2016 Snake fungal disease: an emerging threat to wild snakes. *Phil. Trans. R. Soc. B* **371**, 20150457. (doi:10.1098/rstb.2015.0457)
13. Martel A *et al*. 2014 Recent introduction of a chytrid fungus endangers Western Palearctic salamanders. *Science* **346**, 630–631. (doi:10.1126/science.1258268)
14. Scheele BC *et al*. 2019 Amphibian fungal panzootic causes catastrophic and ongoing loss of biodiversity. *Science* **363**, 1459–1463. (doi:10.1126/science.aav0379)
15. Vredenburg VT, Knapp RA, Tunstall TS, Briggs CJ. 2010 Dynamics of an emerging disease drive large-scale amphibian population extinctions. *Proc. Natl Acad. Sci. USA*. **107**, 9689–9694. (doi:10.1073/pnas.0914111107)
16. Langwig KE, Frick WF, Hoyt JR, Parise KL, Drees KP, Kunz TH, Foster JT, Kilpatrick AM. 2016 Drivers of variation in species impacts for a multi-host fungal disease of bats. *Phil. Trans. R. Soc. B* **371**, 20150456. (doi:10.1098/rstb.2015.0456)
17. Briggs CJ, Knapp RA, Vredenburg VT. 2010 Enzootic and epizootic dynamics of the chytrid fungal pathogen of amphibians. *Proc. Natl Acad. Sci. USA*. **107**, 9695–9700. (doi:10.1073/pnas.0912886107)
18. Grogan LF, Phillott AD, Scheele BC, Berger L, Cashins SD, Bell SC, Puschendorf R, Skerratt LF. 2016 Endemicity of chytridiomycosis features pathogen overdispersion. *J. Anim. Ecol*. **85**, 806–816. (doi:10.1111/1365-2656.12500)
19. Wilber MQ, Langwig KE, Kilpatrick AM, McCallum HI, Briggs CJ. 2016 Integral projection models for host–parasite systems with an application to amphibian chytrid fungus. *Methods Ecol. Evol*. **7**, 1182–1194. (doi:10.1111/2041-210x.12561)
20. Anderson RM, M.May R. 1978 Regulation and stability of host-parasite interactions: I. Regulatory processes. *J. Anim. Ecol*. **47**, 219–247. (doi:10.2307/3933)
21. Lester RJG, McVinish R. 2016 Does moving up a food chain increase aggregation in parasites? *J. R. Soc. Interface* **13**, 20160102. (doi:10.1098/rsif.2016.0102)
22. Valenzuela-Sánchez A, Schmidt BR, Uribe-Rivera DE, Costas F, Cunningham AA, Soto-Azat C. 2017 Cryptic disease-induced mortality may cause host extinction in an apparently stable host–parasite system. *Proc. R. Soc. B* **284**, 20171176. (doi:10.1098/rspb.2017.1176)
23. Hyatt A *et al*. 2007 Diagnostic assays and sampling protocols for the detection of *Batrachochytrium dendrobatidis*. *Dis. Aquat. Org*. **73**, 175–192. (doi:10.3354/dao073175)
24. Miller DAW, Talley BL, Lips KR, Campbell Grant EH. 2012 Estimating patterns and drivers of infection prevalence and intensity when detection is imperfect and sampling error occurs. *Methods Ecol. Evol*. **3**, 850–859. (doi:10.1111/j.2041-210x.2012.00216.x)
25. DiRenzo GV, Campbell Grant EH, Longo AV, Che-Castaldo C, Zamudio KR, Lips KR. 2018 Imperfect pathogen detection from non-invasive skin swabs biases disease inference. *Methods Ecol. Evol*. **9**, 380–389. (doi:10.1111/2041-210x.12868)
26. Grear DA, Hudson P. 2011 The dynamics of macroparasite host-self-infection: a study of the patterns and processes of pinworm (*Oxyuridae*) aggregation. *Parasitology* **138**, 619–627. (doi:10.1017/s0031182011000096)
27. Woodhams DC, Alford RA, Briggs CJ, Johnson M, Rollins-Smith LA. 2008 Life-history trade-offs influence disease in changing climates: strategies of an amphibian pathogen. *Ecology* **89**, 1627–1639. (doi:10.1890/06-1842.1)
28. Johnson PTJ, McKenzie VJ. 2009 Effects of environmental change on helminth infections in amphibians: exploring the emergence of *Ribeiroia* and *Echinostoma* infections in North America. In *The biology of Echinostomes* (eds B Fried, R Toledo), pp. 249–280. New York, NY: Springer Science+Business Media. (doi:10.1007/978-0-387-09577-6_11)
29. Lande R, Engen S, Saether BE. 2003 *Stochastic population dynamics in ecology and conservation*. Oxford, UK: Oxford University Press.
30. Longo AV, Rodriguez D, da Silva Leite D, Toledo LF, Mendoza Almeralla C, Burrowes PA, Zamudio KR. 2013 ITS1 copy number varies among *Batrachochytrium dendrobatidis* strains: implications for qPCR estimates of infection intensity from field-collected amphibian skin swabs. *PLoS ONE* **8**, e59499. (doi:10.1371/journal.pone.0059499)
31. Byrne AQ, Waddle AW, Saenz V, Ohmer M, Jaeger JR, Richards-Zawacki CL, Voyles J, Rosenblum EB. 2022 Host species is linked to pathogen genotype for the amphibian chytrid fungus (*Batrachochytrium dendrobatidis*). *PLoS ONE* **17**, e0261047. (doi:10.1371/journal.pone.0261047)
32. Martins RA *et al*. 2022 Signatures of functional bacteriome structure in a tropical direct-developing amphibian species. *Anim. Microbiome* **4**, 40. (doi:10.1186/s42523-022-00188-7)
33. Wilber MQ, Johnson PTJ, Briggs CJ. 2020 Disease hotspots or hot species? Infection dynamics in multi-host metacommunities controlled by species identity, not source location. *Ecol. Lett*. **23**, 1201–1211. (doi:10.1111/ele.13518)
34. Wilber MQ *et al*. 2022 Once a reservoir, always a reservoir? Seasonality affects the pathogen maintenance potential of amphibian hosts. *Ecology* **103**, e3759. (doi:10.1002/ecy.3759)
35. Bonhoeffer S, Fraser C, Leventhal GE. 2015 High heritability is compatible with the broad distribution of set point viral load in HIV carriers. *PLoS Pathog*. **11**, e1004634. (doi:10.1371/journal.ppat.1004634)
36. Yang Q *et al*. 2021 Just 2% of SARS-CoV-2–positive individuals carry 90% of the virus circulating in communities. *Proc. Natl Acad. Sci. USA*. **118**, e2104547118. (doi:10.1073/pnas.2104547118)
37. Kilpatrick AM, Ives AR. 2003 Species interactions can explain Taylor's power law for ecological time series. *Nature* **422**, 65–68. (doi:10.1038/nature01471)
38. Lagrue C, Poulin R, Cohen JE. 2015 Parasitism alters three power laws of scaling in a metazoan community: Taylor's law, density-mass allometry, and variance-mass allometry. *Proc. Natl Acad. Sci. USA*. **112**, 1791–1796. (doi:10.1073/pnas.1422475112)
39. Knapp RA, Wilber MQ, Joseph MB, Smith TC, Grasso RL. 2024 Reintroduction of resistant frogs facilitates landscape-scale recovery in the presence of a lethal fungal disease. *Nat. Commun*. **15**, 9436. (doi:10.1038/s41467-024-53608-4)
40. Duerr HP, Dietz K. 2000 Stochastic models for aggregation processes. *Math. Biosci*. **165**, 135–145. (doi:10.1016/s0025-5564(00)00014-6)
41. Wilber MQ, Johnson PTJ, Briggs CJ. 2017 When can we infer mechanism from parasite aggregation? A constraint-based approach to disease ecology. *Ecology* **98**, 688–702. (doi:10.1002/ecy.1675)
42. Gaba S, Ginot V, Cabaret J. 2005 Modelling macroparasite aggregation using a nematode-sheep system: the Weibull distribution as an alternative to the negative binomial distribution? *Parasitology* **131**, 03. (doi:10.1017/s003118200500764x)

43. Poulin R. 1993 The disparity between observed and uniform distributions: a new look at parasite aggregation. *Int. J. Parasitol*. **23**, 937–944. (doi:10.1016/0020-7519(93)90060-c)
44. McVinish R, Lester RJG. 2020 Measuring aggregation in parasite populations. *J. R. Soc. Interface* **17**, 20190886. (doi:10.1098/rsif.2019.0886)
45. Knapp RA, Fellers GM, Kleeman PM, Miller DAW, Vredenburg VT, Rosenblum EB, Briggs CJ. 2016 Large-scale recovery of an endangered amphibian despite ongoing exposure to multiple stressors. *Proc. Natl Acad. Sci. USA*. **113**, 11889–11894. (doi:10.1073/pnas.1600983113)
46. Wilber MQ, Knapp RA, Smith TC, Briggs CJ. 2022 Host density has limited effects on pathogen invasion, disease-induced declines and within-host infection dynamics across a landscape of disease. *J. Anim. Ecol*. **91**, 2451–2464. (doi:10.1111/1365-2656.13823)
47. McGill BJ, Nekola JC. 2010 Mechanisms in macroecology: AWOL or purloined letter? Towards a pragmatic view of mechanism. *Oikos* **119**, 591–603. (doi:10.1111/j.1600-0706.2009.17771.x)
48. Wilber MQ, Pfab F, Ohmer MEB, Briggs CJ. 2021 Integrating infection intensity into within- and between-host pathogen dynamics: implications for invasion and virulence evolution. *Am. Nat.* **198**, 661–677. (doi:10.1086/716914)
49. Duerr HP, Dietz K, Eichner M. 2003 On the interpretation of age–intensity profiles and dispersion patterns in parasitological surveys. *Parasitology* **126**, 87–101. (doi:10.1017/s0031182002002561)
50. Jani AJ, A.Knapp R, J.Briggs C. 2017 Epidemic and endemic pathogen dynamics correspond to distinct host population microbiomes at a landscape scale. *Proc. R. Soc. B* **284**, 20170944. (doi:10.1098/rs.2017.0944)
51. Schrock S, Walsman J, DeMarchi J *et al*. 2025 Do fungi look like macroparasites? Quantifying the patterns and mechanisms of aggregation for host-fungal parasite relationships. *Dryad Digital Repository*. (doi:10.5061/dryad.mgqnk998g)
52. Schrock SAR, Walsman JC, DeMarchi JA, LeSage E, Ohmer MEB, Rollins-Smith L *et al*. 2025 Supplementary material from: Do fungi look like macroparasites? Quantifying the patterns and mechanisms of aggregation for host-fungal parasite relationships. Figshare. (doi:10.6084/m9.figshare.c.7667272)